

# The Influence of Vascular Morphology on DSC-MRI Derived Blood Volume Measurements in Brain Tumors

Natanael B Semmineh<sup>1</sup>, Junzhong Xu<sup>1</sup>, and C. Chad Quarles<sup>1</sup>

<sup>1</sup>Institute of Imaging Science, Vanderbilt University, Nashville, TN, United States

**Target Audience:** Clinicians and basic scientists who apply and investigate DSC-MRI methods in patients with brain tumors.

**Purpose:** A central assumption in all DSC-MRI studies is that a linear relationship, with a spatially uniform rate constant, termed the vascular susceptibility calibration factor ( $K_p$ ), exists between the contrast agent (CA) concentration and the measured transverse relaxation rate change. Given the dependence of susceptibility field gradients on vascular morphology, this assumption could influence DSC-MRI hemodynamic measurements. Whereas vascular networks in normal tissue are highly ordered, those found in tumors are abnormally heterogeneous, with a large degree of random variation in vessel length, diameter and branching patterns. In this computational study, we investigate the influence of vascular morphology on DSC-MRI derived blood volume measurements and characterize the vascular susceptibility calibration factor for arbitrary vascular tree networks that replicate structural properties observed in normal and tumor tissue.

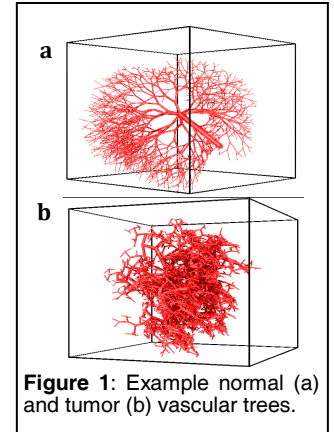


**Figure 1:** Example normal (a) and tumor (b) vascular trees.

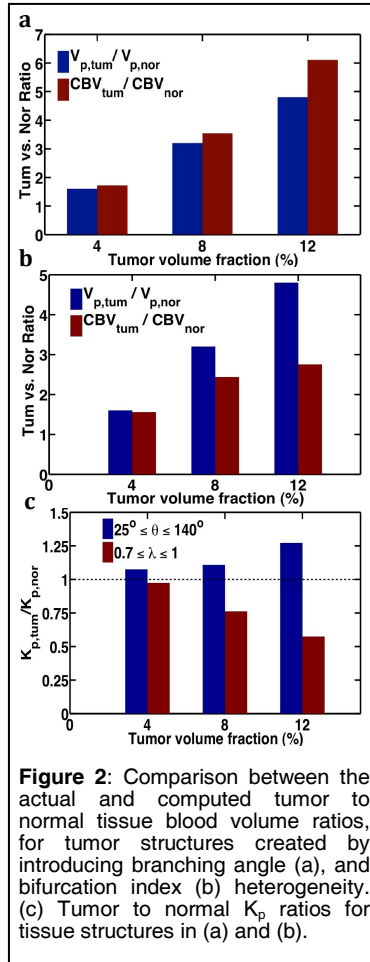


**Figure 2:** Comparison between the actual and computed tumor to normal tissue blood volume ratios, for tumor structures created by introducing branching angle (a), and bifurcation index (b) heterogeneity. (c) Tumor to normal  $K_p$  ratios for tissue structures in (a) and (b).

**Methods:** To simulate susceptibility contrast induced by CA compartmentalization within arbitrary shaped vascular networks, we used an approach termed the Finite Perturber Finite Difference Method [1]. Vascular networks were created using a fractal tree model [2]. Starting with an initial cylindrical segment representing an arterial vessel, the vascular tree is created using bifurcation and trifurcation at each junction into smaller daughter segments. Normal vascular trees were created using a volume fraction of 2.5%, while a range of volume fractions (4%, 8% and 12%) were used for tumor structures. For the tumor structures, heterogeneity was introduced by increasing the variability of two parameters, the bifurcation index ( $\lambda$ ), which is the ratio of daughter vessel diameters, and the branching angle between the daughter vessels ( $\theta$ ). A dose response curve was simulated in order to compute  $K_p$  for each structure. Contrast agent concentration and the associated  $\Delta R2^*$  time courses were also simulated. Cerebral blood volume (CBV) values for the normal and tumor structures were computed as the area under the computed  $\Delta R2^*$  time course.

**Results:** Figure 1 shows an example symmetric “normal” vascular tree featuring a homogenous set of input parameters and a more heterogeneous “tumor” like structure. The computed rCBV values ( $CBV_{tum}/CBV_{nor}$ ) along with the actual vascular volume fraction ratios ( $V_{p,tum}/V_{p,nor}$ ) for three tumor like tissue structures with volume fractions of 4%, 8% and 12% are shown in Figures 2a and 2b. The results in Figure 2a are for tumor tissue structures obtained by introducing a wider branching angle heterogeneity ( $25^\circ \leq \theta \leq 140^\circ$ ) at each bifurcation node compared to the narrow branching angle range ( $25^\circ \leq \theta \leq 40^\circ$ ) used to create the normal tissue structure. As the tumor vascular volume fraction increases the difference between the computed rCBV and the actual vascular volume fraction ratio increases from 6.9% to 21.3%. Figure 2b shows results for tumor tissue structures constructed by increasing bifurcation index heterogeneity ( $0.7 \leq \lambda \leq 1$ ). As variation in  $\lambda$  increases, the rCBV underestimates the actual vascular volume fraction ratio to a greater degree, with the differences ranging from 2.7% to 74.3%. These opposing results are summarized using the ratio of the tumor to normal tissue vascular susceptibility calibration factor ( $K_{p,tum}/K_{p,nor}$ ) as shown in Figure 2c. Increasing branching angle heterogeneity tended to increase tumor  $K_p$  values, whereas increasing bifurcation index heterogeneity decreased  $K_p$ , with the latter effect being more predominant. It is of note that the difference in normal and tumor  $K_p$  values for the bifurcation index heterogeneity case, with a 12% blood volume fraction, agrees closely with previously reported *in vivo* data in 9L brain tumors [3].

**Discussion:** The preliminary computational results presented herein show marked  $K_p$  heterogeneity across vascular networks, suggesting that the assumption of a constant  $K_p$  for all tissue types could affect DSC-MRI derived perfusion parameters. However, it is encouraging that morphological features can both increase and decrease tumor  $K_p$  values, as this may suggest that the net effect *in vivo* is less substantial than observed herein due to averaging. Also, the highly abnormal  $K_p$  values reported here only occurred in vascular trees that possessed exceptionally high vascular volume fraction ratios (~5). Currently a more stringent study is under way to characterize  $K_p$  for wider range of simulated vascular trees as well as  $\mu$ CT based tissue angiograms.

**Conclusion:** While  $K_p$  heterogeneity may have little clinical impact on identifying highly vascular tumors it could affect the interpretation of serial DSC-MRI data during treatment response. Treatment induced changes in the vascular network, such as that observed with anti-angiogenic treatment, could serially alter  $K_p$  values. Further studies are needed to explore this effect and suggest the need to validate serial DSC-MRI measurements of tumor hemodynamics.

**References:** [1] Semmineh N., et al., ISMRM 2010. [2] E. Sabo, et al., Clin Cancer Res, vol. 7, no. 3, pp. 533–7, Mar 2001. [3] Pathak A. P., et al. J. MRI 18:397–403 (2003).

**Acknowledgements:** NCI R00 CA127599, NCI R01 CA158079, NCI P30 CA068485, NCI U24 CA126588